tvst

https://doi.org/10.1167/tvst.7.5.5

Article

Ultrasound Imaging and Measurement of Choroidal Blood Flow

Raksha Urs[1], Jeffrey A. Ketterling[2], Alfred C. H. Yu[3], Harriet O. Lloyd[1], Billy Y. S. Yiu[3], and Ronald H. Silverman[1]

[1] Department of Ophthalmology, Columbia University Medical Center, New York, NY, USA
[2] F.L. Lizzi Center for Bioengineering, Riverside Research, New York, NY, USA
[3] Department of Electrical and Computer Engineering, University of Waterloo, Waterloo, ON, Canada

Correspondence: Ronald H. Silverman, Department of Ophthalmology, Columbia University Medical Center, 635 W 165th St, Room 711, New York, NY 10032, USA. e-mail: rs3072@cumc.columbia.edu

Received: 9 January 2018
Accepted: 30 July 2018
Published: 4 September 2018

Keywords: choroid; ultrasound; blood-flow

Citation: Urs R, Ketterling JA, Yu ACH, Lloyd HO, Yiu BYS, Silverman RH. Ultrasound imaging and measurement of choroidal blood flow. Trans Vis Sci Tech. 2018;7(5):5, https://doi.org/10.1167/tvst.7.5.5

Purpose: The choroid is a vascular network providing the bulk of the oxygen and nutrient supply to the retina and may play a pivotal role in retinal disease pathogenesis. While optical coherence tomography angiography provides an en face depiction of the choroidal vasculature, it does not reveal flow dynamics. In this report, we describe the use of plane-wave ultrasound to image and characterize choroidal blood flow.

Methods: We scanned both eyes of 12 healthy subjects in a horizontal plane superior to the optic nerve head using an 18-MHz linear array. Plane-wave data were acquired over 10 transmission angles that were coherently compounded to produce 1000 images/sec for 3 seconds. These data were processed to produce a time series of power Doppler images and spectrograms depicting choroidal flow velocity. Analysis of variance was used to characterize peak systolic, and end diastolic velocities and resistive index, and their variability between scans, eyes, and subjects.

Results: Power Doppler images showed distinct arterioles within a more diffuse background. Choroidal flow was moderately pulsatile, with peak systolic velocity averaging approximately 10 mm/sec and resistive index of 0.55. There was no significant difference between left and right eyes, but significant variation among subjects.

Conclusions: Plane-wave ultrasound visualized individual arterioles and allowed measurement of flow over the cardiac cycle. Characterization of choroidal flow dynamics offers a novel means for assessment of the choroid's role in ocular disease.

Translational Relevance: Characterization of choroidal flow dynamics offers a novel means for assessment of the choroid's role in ocular disease.

Introduction

The retina has one of the highest metabolic demands of any tissue[1,2] requiring a rich supply of oxygen and other nutrients. While the central retinal artery provides the inner retina's blood supply, most of its oxygen demand is supplied by diffusion from the underlying choroid (which is the sole supply of the avascular fovea), which is in turn supplied by the ciliary arteries. While choroidal changes are associated with retinal diseases, such as age-related macular degeneration[3] and diabetic retinopathy,[4,5] the limited ability to characterize choroidal flow leaves its role in pathogenesis and progression unclear.

The choroid has the highest rate of blood flow per unit weight of any tissue.[6] Sandwiched between the retinal pigment epithelium (RPE) and the sclera, the choroid is approximately 0.22- to 0.3-mm thick at the posterior pole, thinning anteriorly. Aside from Bruch's membrane, which is the choroid's innermost layer lying beneath the RPE, the choroid is traditionally divided into the following three layers: the choriocapillaris, a flat network of anastomosed capillaries beneath Bruch's membrane; Sattler's layer, comprising medium-sized vessels; and Haller's layer,

the outermost layer comprised of larger vessels. Note, however, that there is really no distinct interface between layers, especially Sattler's and Haller's.

Because the choroid is sandwiched between the light-absorbing RPE and the optically opaque sclera, it is more difficult to image than the optically accessible retina. Until recently, indocyanine green (ICG) angiography[7,8] was the primary technique available for imaging choroidal flow in vivo. With an optical absorption band from approximately 750 to 800 nm and a somewhat longer fluorescence emission wavelength, ICG allows imaging using near infrared light that can penetrate the RPE. ICG angiography can demonstrate leaking or blocked choroidal vessels and other vascular abnormalities. But while ICG angiography can provide en face images over time depicting the pattern of choroidal filling as the dye perfuses the choroid, it cannot provide information regarding flow velocity or dynamics over the cardiac cycle.

Laser Doppler flowmetry[9] uses a weakly focused 800-nm diode laser beam delivered via a fundus camera to provide point measurements of choroidal flow, primarily the choriocapillaris, in the region of the fovea, where more superficial retinal vessels that would otherwise obscure the signal are absent. Because the technique is limited to the fovea, it is unable to provide information regarding pathologic changes in choroidal flow not specific to this region.

Laser speckle flowgraphy[10,11] uses a scanned laser beam to acquire multiple fundus images over time from which mean blur rate (in arbitrary units), a proxy for flow velocity, is determined at each point. Like laser Doppler flowmetry, however, this method is affected by the presence of overlying retinal vessels, limiting evaluation of the choroid to regions where retinal vessels are absent.

Early time-domain optical coherence tomography (OCT) technology had very limited capacity to penetrate beyond the RPE, but the increased sensitivity provided by spectral-domain technology, especially the enhanced-depth imaging method described by Spaide[12] using the conjugate image, allows structural imaging of the choroid. Swept-source OCT, operating at a 1-μm wavelength, has also been very effective in choroidal imaging because of the improved light penetration of the RPE at this longer wavelength.[13]

Several phase- or Doppler-[14,15] and speckle-based methods[16,17] for retinal and choroidal OCT angiography (OCT-A) have been described. OCT-A essentially thresholds speckle decorrelation over time at each point in an en face representation of the retina and choroid at specific depths.[18] Regional perfusion can be characterized as the percentage of a region of interest (e.g., the macula) occupied by vessels with flow above the detection threshold. Using the split-spectrum amplitude-decorrelation method,[19] it is also possible to calculate flow index, defined as the average decorrelation value in the peripapillary region of the en face retinal angiogram.

Ultrasound Doppler methods have long been used to demonstrate and measure blood flow in the retrobulbar vessels supplying the eye. Clinical use, however, has been limited because most commercial linear-array ultrasound systems exceed Food and Drug Administration (FDA) guidelines for ophthalmic diagnostic ultrasound intensity.

In conventional ultrasound linear-array imaging, groups of adjacent array elements (arrays typically consist of 64–256 elements) emit a focused beam and the return echoes are received and beamformed by the same or additional elements to form one image line. This process is iterated from one side of the array to the other to form one B-mode image. This process is time consuming and limits the maximum frame rate that can be achieved.

A recently developed approach to overcome these limitations is plane-wave imaging,[20] in which all array elements emit together to form one unfocused, steered wavefront. Echoes are received by all array elements and high-speed beamforming of echo data by computer processing permits one image to be generated from one transmit event. This technique allows imaging at the maximum pulse repetition frequency (PRF), and allows imaging frame rates as much as 100× faster than a conventionally scanned linear array and 1000× faster than a mechanically scanned ophthalmic B-scanner. For the posterior pole of the eye, the two-way pulse/echo transit time is approximately 30 μsec, which would allow a PRF of up to 33 kHz, although other factors, including the need to acquire sufficient data from each array element, limit the maximum PRF to approximately 23 kHz. The summation (i.e., compounding) of plane-wave frames acquired at different transmit angles is an enhancement of the technique, improving signal-to-noise ratio (SNR) and lateral resolution.[21] With compounding of N angles, however, the imaging rate is reduced to a maximum of PRF/N.

Because plane-wave transmission does not produce a focused beam, ultrasound intensity is substantially reduced compared with conventionally scanned linear arrays, and we have shown that plane-wave imaging,

including Doppler, can be readily performed while complying with stringent FDA ophthalmic standards.[22]

Characterization of choroidal flow is especially challenging because of the low resolution of ultrasound compared with OCT, the small luminal diameters of choroidal vasculature (~25 μm for the arterioles and venules and <10 μm for the flattened, ovoid vessels of the choriocapillaris[23]), the slow flow compared with vessels supplying the retina and choroid (the central retinal and ciliary arteries), and the direction of flow, which is normal to the ultrasound axis in the choriocapillaris.

In this report, we describe methods addressing the above issues to allow visualization of choroidal arterioles and measurement of choroidal flow velocities over the cardiac cycle. Our previous report[24] emphasized imaging at a sufficiently high PRF to characterize high-flow velocities in the major retrobulbar vessels. In this report, we describe refinements aimed at improving sensitivity to slow flow, specifically acquisition of compound data at a high PRF (23 kHz; to minimize motion-induced blurring) while storing long temporal sequences of compounded data at a lower PRF (1 kHz) to facilitate sensitivity to slow flow. To our knowledge, this is the first report on human choroidal blood-flow dynamics using ultrasound.

Materials and Methods

We acquired all data with a Verasonics Vantage 128 (Verasonics, Inc., Kirkland, WA) ultrasound engine, which is a programmable ultrasound research platform. We used a Verasonics L22-14v linear array transducer, which has an 18-MHz center frequency (~80-μm wavelength) and an elevation focal length of 18 mm. We developed MATLAB (MathWorks, Natick, MA) programs to control transmit and receive of all transducer elements to emit plane waves at multiple angles and to beamform echo data to produce compound images. Phase-resolved echo data received by the linear-array transducer elements were quadrature sampled at 62.5 MHz at 14-bits per sample.

Acoustic intensity measurements under the experimental conditions of excitation were performed with a certified, calibrated 40-μm diameter needle hydrophone (Precision Acoustics, Inc., Dorset, UK) as previously reported.[24] In the focal plane, the derated spatial-peak pulse average intensity was 3.0 W/cm^2, spatial-peak temporal average intensity was 7.0 mW/cm^2, and mechanical index was 0.07. The FDA ophthalmic limits for these parameters are 28 W/cm^2, 17 mW/cm^2, and 0.23, respectively.[25]

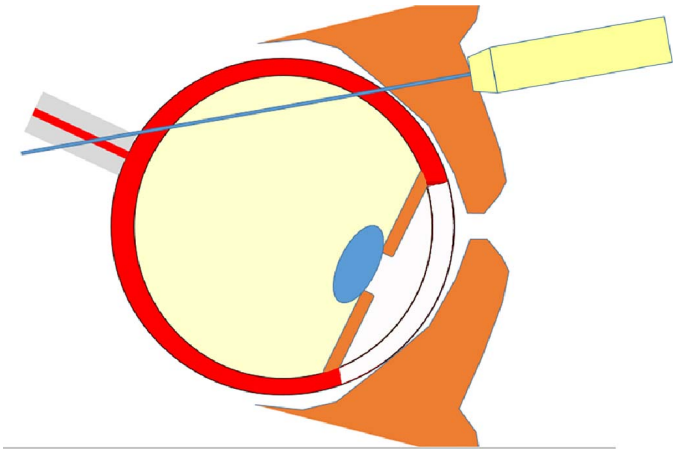

Figure 1. Schematic illustrating the orientation of the ultrasound probe and the eye during scanning. The probe was placed against the closed upper lid and the scan plane (*blue line*) crossed the choroid somewhat obliquely in a horizontal plane superior to the optic nerve.

Clinical Imaging Setup

The study followed the principles of the Declaration of Helsinki. Informed consent was obtained under a research protocol approved by the Institutional Review Board/Ethics Committee.

Scans were performed through the closed eyelid with the subject in a seated position looking forward or slightly downward. After application of gel (GenTeal; Alcon Laboratories Inc., Fort Worth, TX) on the probe surface to provide acoustic coupling to the eyelid, the upper edge of the horizontally oriented probe was positioned against the superior frontal orbital bone. The optic nerve was then located using a duplex, real-time imaging mode and the probe tilted to position the scan plane just superior to the optic nerve head (ONH). After acquiring data continuously for 3 seconds, the probe was removed from the eye and data stored (taking ~10 seconds). The process was then repeated twice and then the other eye was similarly examined for a total of three scans per eye. A schematic illustrating the scan geometry is provided in Figure 1.

Twelve healthy subjects were examined, with three scans of both eyes acquired in one session. Subjects (6 male, 6 female) had no history of eye disease and ranged in age from 26 to 67 years (mean 39.1, SD = 14.2).

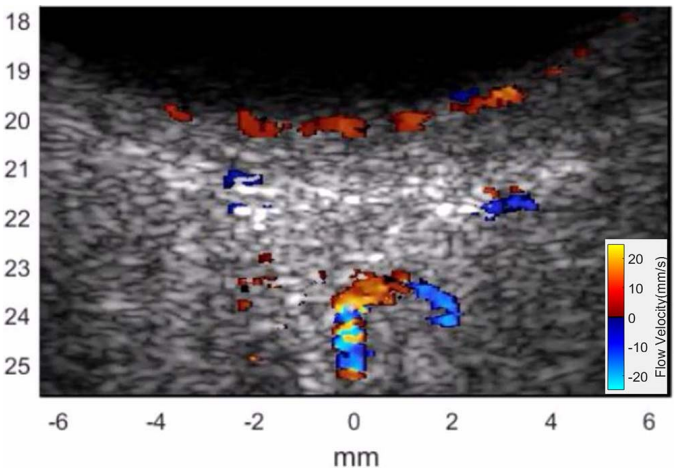

Figure 2. Real-time B-mode image with 'flash Doppler' color flow superimposed. The image depicts choroidal flow at systole. At diastole, choroidal flow was generally undetected in this mode. Because the scan plane cuts through the optic nerve as illustrated in Figure 1, flow in the central retinal artery and/or the short posterior ciliary arteries appears in the orbit.

Technical Setup

A two-mode custom MATLAB program was developed for image acquisition.[25] In 'flash Doppler' mode (Fig. 2), B-mode images with color-flow Doppler superimposed were displayed real time. This mode was used to interactively position the scan plane in the region of interest. Although flash Doppler images have lower sensitivity and resolution for flow than obtained after postprocessing, they typically demonstrated choroidal vessels and pulsatility.

In the second, high-resolution mode, batches of 10 plane waves were transmitted at equal angular increments over ±9° at a PRF of 23 kHz, the fastest possible rate given the two-way acoustic transit time. Batches were transmitted at 1-msec intervals for 3 seconds and data stored for postprocessing. Postprocessing consisted of beamforming and coherent compounding (i.e., with phase information retained) of each batch to form a single compound image. Three thousand phase-resolved compound images were thus formed at 1-msec intervals (1 kHz) over the 3-second acquisition period.

Postprocessing was as follows: the data were initially processed using a singular value decomposition (SVD) filter[26] followed by a 10-Hz high-pass filter. The SVD filter exploits the different spatial coherence characteristics of bulk tissue motion caused by movement of the eye or the hand-held probe versus blood flow, even when their velocities are comparable. Whereas bulk tissue motion is uniform in direction (high coherence), blood flow varies in direction and velocity with vessel anatomy and orientation. The 10-Hz high-pass filter sets a threshold of approximately 0.5 mm/sec for minimum detectable velocity and acts to improve distinction of flow from noise.

A 64-msec long spatiotemporal sliding-window was used to produce a time-series of images demonstrating flow variation over the 3-second period of data acquisition. Summing the intensities from the blood-flow signal then produced power-Doppler images. The power-Doppler image time series was then manually segmented to allow generation of spectrograms representing the flow velocity of the whole choroid within the scan plane as a function of time. After application of phase unwrapping to the spectrogram to compensate for potential aliasing (which would occur for velocities >21 mm/sec under the experimental conditions), the envelope of the spectrogram was automatically detected.[27] The peak systolic velocity (PSV), end diastolic velocity (EDV) and average velocity (V_{MEAN}) in two successive cardiac cycles were measured and the resistive index (RI) calculated as RI = (PSV − EDV) / PSV.

Statistical Analysis

We averaged PSV, EDV, and RI on two successive cycles in each of the triplicate scans of each eye. Analysis of variance (ANOVA) was performed to characterize variation within triplicate scans of each eye, between left and right eyes and between subjects.

Results

Figure 2 is a typical real-time flash-Doppler image, taken at systole, of the posterior of the eye in a horizontal plane just superior to the ONH. At diastole, the color-flow signal from the choroid is almost entirely absent. Note that the choroidal flow detected in this image is not contiguous, but rather appears in discrete areas separated by tissue in which flow is undetected.

Figure 3 shows the appearance of a postprocessed scan centered on the ONH. In this image, orbital vessels, including the central retinal artery and short posterior ciliary artery, are visualized. Flow in the choroid is contiguous. Retinal flow is also seen.

Figure 4 demonstrates choroidal flow in a horizontal plane superior to the ONH, the standard orientation used in this study. In this case, the choroid was imaged at a somewhat oblique incidence, which has the effect of elongating the choroid with respect to

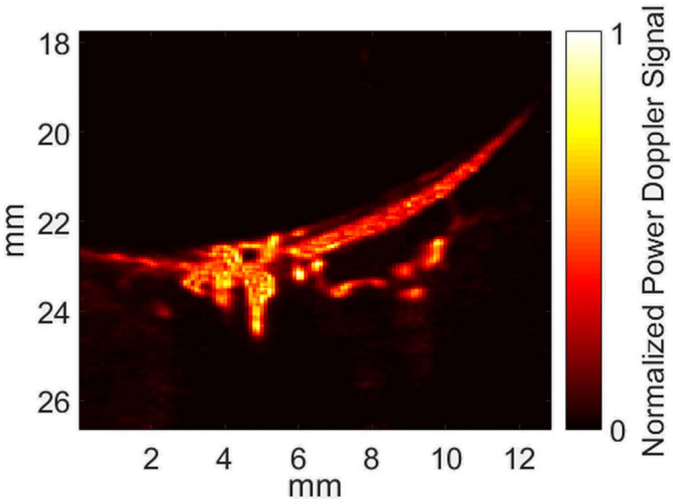

Figure 3. High-resolution power Doppler image centered on the optic nerve head. In this orientation, choroidal and retinal flow as well as orbital vasculature were visualized.

the ultrasound imaging plane. The velocity image shows relatively little spatial velocity variation within the choroid at systole, although somewhat higher velocities are present in the peripapillary region where arterial flow enters the choroid. The power-Doppler image shows the choroidal flow to consist of an unresolved background component with vessels oriented roughly in a posterior-to-anterior direction, but progressively more oblique with distance from the ONH. Qualitatively, most scans showed distinct choroidal vessels as seen in Figure 4. The spectrogram of the total choroid in the scan plane shows pulsatile arterial flow, but with some venous flow (i.e., having negative flow velocities), which appear to be less than 3 mm/s. In this instance, a PSV of approximately 12 mm/s was observed. Note, however, that spectrograms depict a range of velocities present in the analysis region. The velocity value at any point is defined as the upper limit of the spectrogram envelope. In contrast, power-Doppler magnitude is the area under the spectrogram envelope. Consequently, power-Doppler images have a higher SNR than velocity images.

Quantitative measures of flow for the study population are summarized in the Table. The coefficients of variation among triplicate scans within eyes were 18.5% for PSV, 33.0% for EDV, 20.3% for V_{MEAN}, and 17.4% for RI. ANOVA showed significant variation between subjects for PSV ($P < 0.001$), V_{MEAN} ($P = 0.013$), and RI ($P < 0.001$) but no significant difference for any parameter between right and left eyes.

Discussion

We previously demonstrated the use of ultrafast plane-wave ultrasound to image and measure flow in the major vessels supplying the eye.[25] In this report, we modified our previous fast-flow (>50 mm/sec) method that was used to characterize flow in the central retinal and posterior ciliary arteries. To improve sensitivity to slow flow, we increased the number of compounded angles per image and reduced the acquisition rate of coherently compounded frames from 6.7 kHz for fast flow in the major retrobulbar vessels to 1 kHz for the choroid. At this slower acquisition rate, velocities only up to 21 mm/s could be measured without resorting to phase-unwrapping

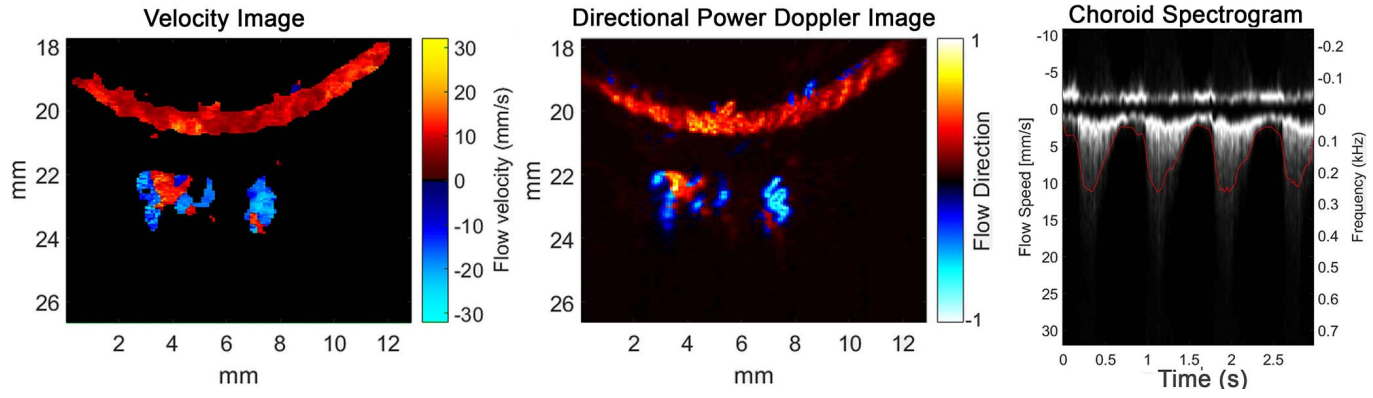

Figure 4. Blood flow in a horizontal plane cutting obliquely through the choroid superior to the ONH, as depicted schematically in Figure 1. *Left*: systolic velocity image shows relatively little spatial variation within the choroid with exception of higher velocities in the central, peripapillary region. *Center*: power-Doppler image resolving individual choroidal arterioles. *Right*: spectrogram of full choroid capturing four cardiac cycles, with a PSV of approximately 12 mm/sec.

Table. Mean Values and Standard Deviations of Choroidal Flow Parameters of 24 Eyes of 12 Subjects

	PSV, mm/s	EDV, mm/s	Vmean, mm/s	RI
Right eyes	10.35 ± 2.01	4.48 ± 0.88	6.71 ± 1.05	0.543 ± 0.136
Left eyes	9.89 ± 2.72	4.18 ± 0.85	6.51 ± 1.17	0.546 ± 0.162

strategies to compensate for aliasing, but choroidal flow velocities generally do not exceed this value. The reduced acquisition rate, however, improves sensitivity to slow flow. Another difference is that we acquired and coherently added 10 angled plane wave scans for each slow-flow compound image versus just two or three angles for fast flow. The increase in the number of plane waves per compound image results in an improved SNR. Also, by acquiring each set of 10 angled plane waves at the highest possible PRF, potential blurring was reduced. A limitation for detection of very slow flow (≤0.5 mm/sec), however, is imposed by the use of a high-pass filter.

We found that choroidal vessels are most readily visualized when scanning the choroid at a somewhat oblique angle. The overall appearance of the vessels suggests that we are detecting flow in the large arterioles of Sattler's and Haller's layers. Because Doppler methods are most sensitive to flow oriented parallel to the ultrasound axis, flow within these vessels is consistent with generation of a Doppler signal. The thinness and approximately normal orientation of the choriocapillaris to the ultrasound axis would be expected to produce little Doppler signal.

We found data quality to be dependent on a steady hand and minimal eye motion over the 3 seconds of data acquisition. Data quality can be assessed by immediate review and the scan repeated if motion is evident.

Another limitation we encountered was in evaluation of high myopes, none of which were included in the subject cohort. Because the probe has a fixed focus in the elevation axis of approximately 18 mm, this reduces resolution and sensitivity in axial myopes.

Velocity values presented in this report do not include correction of flow angle with respect to the ultrasound axis. While this is standard for Doppler flow velocity determinations in large vessels whose orientation can be readily determined, it would be challenging to apply this to the choroid, where arterioles and capillaries are short in length and tortuous in conformation. The reported velocity values can therefore be treated as a lower bound for actual velocities. The application of vector flow techniques, however, may offer an avenue toward addressing this issue.[28]

In conclusion, we demonstrated visualization and measurement of blood flow and pulsatility over the cardiac cycle in the choroid in a small cohort of healthy subjects and described normative values and variability. This technique may now be applied to a larger cohort, taking into account demographic factors, such as age and sex. Other factors, such as patient position (seated versus supine), should also be explored. Finally, the method will be of great interest when applied to disease conditions, such as age-related macular degeneration, diabetic retinopathy, glaucoma, and choroidal tumors, where it can provide information on flow dynamics complementary to the en face structural presentation of the choroidal vasculature provided by OCT-A.

Acknowledgments

Supported by grants from the National Institutes of Health Grants EY025215, EY028550, and P30 EY019007 (Core Facilities for Vision Research) and an unrestricted grant to the Department of Ophthalmology of Columbia University from Research to Prevent Blindness.

Disclosure: **R. Urs**, None; **J.A. Ketterling**, None; **A.C.H. Yu**, None: **H.O. Lloyd**, None; **B.Y.S. Yiu**, None; **R.H. Silverman**, None

References

1. Yu DY, Cringle SJ. Oxygen distribution and consumption within the retina in vascularised and avascular retinas and in animal models of retinal disease. *Prog Retin Eye Res*. 2001;20:175–208.
2. Cohen LH, Noell WK. Relationships between visual function and metabolism. In: Graymore

CN, ed. *Biochemistry of the Retina*. Orlando: Academic Press Inc.; 1965;36–50.
3. Ferrara D, Silver RE, Louzada RN, et al. Optical coherence tomography features preceding the onset of advanced age-related macular degeneration. *Invest Ophthalmol Vis Sci*. 2017;58:3519–3529.
4. Langham ME, Grebe R, Hopkins S, Marcus S, Sebag M. Choroidal blood flow in diabetic retinopathy. *Exp Eye Res*. 1991;52:167–173.
5. Adhi M, Brewer E, Waheed NK, Duker JS. Analysis of morphological features and vascular layers of choroid in diabetic retinopathy using spectral-domain optical coherence tomography. *JAMA Ophthalmol*. 2013;131:1267–1274.
6. Alm A, Bill A. Ocular and optic nerve blood flow at normal and increased intraocular pressures in monkeys (Macacairus): a study with radioactively labelled microspheres including flow determinations in brain and some other tissues. *Exp Eye Res*. 1973;15:15–29.
7. Flower RW, Hochheimer BF. Clinical infrared absorption angiography of the choroid [letter]. *Am J Ophthalmol*. 1972;73:458.
8. Stanga PE, Lim JI, Hamilton P. Indocyanine green angiography in chorioretinal diseases: indications and interpretation. *Ophthalmology*. 2003;110:15–24.
9. Riva CE, Cranstoun SD, Grunwald JE, et al. Choroidal blood flow in the foveal region of the human ocular fundus. *Invest Ophthalmol Vis Sci*. 1994;35:4273–81
10. Tamaki Y, Araie M, Kawamoto E, et al. Noncontact, two-dimensional measurement of retinal microcirculation using laser speckle phenomenon. *Invest Ophthalmol Vis Sci*. 1994;35:3825–3834.
11. Kunikata H, Nakazawa T. Recent clinical applications of laser speckle flowgraphy in eyes with retinal disease. *Asia Pac J Ophthalmol*. 2016;5:151–158.
12. Spaide RF, Koizumi H, Pozzoni MC. Enhanced depth imaging spectral-domain optical coherence tomography. *Am J Ophthalmol*. 2008;146:496–500.
13. Unterhuber B, Povazay B, Hermann H. In vivo retinal optical coherence tomography at 1040 nm-enhanced penetration into the choroid. *Opt Express*. 2005;13:3252–8.
14. Hong YJ, Makita S, Jaillon F, et al. High-penetration swept source Doppler optical coherence angiography by fully numerical phase stabilization. *Opt Express*. 2012;20:2740–60.
15. Fingler J, Zawadzki RJ, Werner JS, et al. Volumetric microvascular imaging of human retina using optical coherence tomography with a novel motion contrast technique. *Opt Express*. 2009;17:22190–200.
16. Hendargo HC, Estrada R, Chiu SJ, et al. Automated non-rigid registration and mosaicing for robust imaging of distinct retinal capillary beds using speckle variance optical coherence tomography. *Biomed Opt Express*. 2013;4:803–21.
17. Jonathan E, Enfield J, Leahy MJ. Correlation mapping method for generating microcirculation morphology from optical coherence tomography (OCT) intensity images. *J Biophotonics*. 2011;4:583–7.
18. Yu S, Lu J, Cao D, et al. The role of optical coherence tomography angiography in fundus vascular abnormalities. *BMC Ophthalmology*. 2016;16:107.
19. Jia Y, Tan O, Tokayer J, et al. Split-spectrum amplitude-decorrelation angiography with optical coherence tomography. *Opt Express*. 2012;20:4710–25.
20. Tanter M, Fink M. Ultrafast imaging in biomedical ultrasound. *IEEE Trans Ultrason Ferroelectr Freq Control*. 2014;61:102–119.
21. Tanter M, Bercoff J, Sandrin L, Fink M. Ultrafast compound imaging for 2-D motion vector estimation: application to transient elastography. *IEEE Trans Ultrason Ferroelectr Freq Control*. 2002;49:1363–1374.
22. Urs R, Ketterling JA, Silverman RH. Ultrafast ultrasound imaging of ocular anatomy and blood flow. *Invest Ophthalmol Vis Sci*. 2016:57:3810–3186.
23. Ramrattan RS, van der Schaft TL, Mooy CM, et al. Morphometric analysis of Bruch's membrane, the choriocapillaris, and the choroid in aging. *Invest Ophthalmol Vis Sci*. 1994;35:2857–2864.
24. Ketterling JA, Urs R, Silverman RH. In vivo imaging of ocular blood flow using high-speed ultrasound. *IEEE Int Ultrason Symp*. 2016;2016.
25. Food and Drug Administration. *Information for Manufacturers Seeking Marketing Clearance of Diagnostic Ultrasound Systems and Transducers*. Rockville, MD: Center for Devices and Radiological Health, Food and Drug Administration, US Department of Health and Human Services; 2008.
26. Demene C, Deffieux T, Pernot M, et al. Spatiotemporal clutter filtering of ultrafast ultrasound data highly increases Doppler and fUltrasound sensitivity. *IEEE Trans Med Imaging*. 2015;34:2271–2285.

27. Kathpalia A, Karabiyik Y, Simensen B, et al. A robust Doppler spectral envelope detection technique for automated blood flow measurements. *IEEE Int Ultrason Symp*. 2015;2015.

28. Yiu BYS, Lai SSM, Yu ACH. Vector projectile imaging: time-resolved dynamic visualization of complex flow patterns. *Ultra Med Biol*. 2014;40: 2295–2309.